Phytochemistry 190 (2021) 112856

Contents lists available at ScienceDirect

Phytochemistry

journal homepage: www.elsevier.com/locate/phytochem

Molecular networking-driven isolation of 8′-Glycosylated biscoumarins from *Cruciata articulata*

Xueling Liu [a], Yuyu Dong [a], Valida Alizade [b], Manana Khutsishvili [c], Daniel Atha [d], Robert P. Borris [a], Benjamin R. Clark [a,*]

[a] School of Pharmaceutical Science and Technology, Health Sciences Platform, Tianjin University, Tianjin, 300072, China
[b] Institute of Botany, Azerbaijan National Academy of Sciences, Baku, AZ1102, Azerbaijan
[c] National Herbarium of Georgia, Ilia State University, Tbilisi, 100995, Georgia
[d] New York Botanical Garden, Bronx, NY, USA

ARTICLE INFO

Keywords:
Cruciata articulata
Rubiaceae
Structural elucidation
Molecular networking
Biscoumarins
MS/MS

ABSTRACT

A molecular networking-guided phytochemical investigation of *Cruciata articulata* led to the isolation of five unreported biscoumarins, four of which were characterized by a shared 6-methoxy-7,8′-dihydroxy-3,7′-biscoumarin aglycone. These were isolated alongside two known coumarin glycosides, daphnetin-8-*O*-β-D-glucoside and 6′-acetoxy-daphnetin-8-*O*-β-D-glucoside. Their structures were elucidated by extensive 1D and 2D NMR experiments, in combination with chemical transformation and MS/MS fragmentation analysis. Four of the biscoumarins were glycosylated at the 8′ position: these are the first examples of this substitution pattern to be described in nature. All compounds were tested for cytotoxic, antimicrobial, anti-inflammatory, and α-glucosidase inhibitory properties, but did not display significant activity.

1. Introduction

Cruciata articulata (L.) Ehrend (Rubiaceae) has a range of distribution including Egypt, the Mediterranean region, and western Asia (Abdel-Khalik and Bakker., 2007). Even though volatile oils, coumarins, iridoids, flavonoids and terpenoids have been investigated in the genus *Cruciata* (De Rosa et al., 2003, 2002; Ergun et al., 1984; Il'Ina et al., 2013; Mitova et al., 1996; Tava et al., 2020), only a single phytochemical investigation has focused on *Cruciata articulata*, describing the isolation of anthraquinones from the species (Ushakov et al., 1988).

Coumarins are specialized metabolites widely distributed in plants, especially in the Umbelliferae, Fabaceae, Asteraceae, and Thymelaeaceae families (Gaber et al., 2019; Hoult and Payá., 1996). Coumarins are primarily biogenetically derived from shikimic acid pathways, though a significant amount of them are formed from mixed biosynthetic routes (Knaggs, 2003). Previous reports have demonstrated that coumarins possess a wide range of biological properties (Liang et al., 2011; Pierson et al., 2010), including antibacterial (da Cunha et al., 2020), anticancer (Song et al., 2020), anticoagulant (Greaves, 2005), HIV inhibitory (Liu et al., 2020), antiviral (Mishra et al., 2020), antiglycation (Salar et al., 2019) and anti-inflammatory (Chougala et al., 2018) properties. Additionally, both natural and synthetic coumarins can be used as fluorescent probes or luminescent materials (Jiang et al., 2020; Mahapatra et al., 2013).

Over the past decade, analysis of MS/MS fragmentation patterns has become increasingly useful in the identification of plant metabolites from multiple structure classes (Aron et al., 2020; Gangopadhyay et al., 2016; Wang et al., 2014; M. Watrous et al., 2012). Furthermore, MS/MS molecular networking (MN) has emerged as a promising technique for analyzing LC-based mass spectrometry and metabolomics data sets based on its accessibility through the Global Natural Product Social Network (GNPS; https://gnps.ucsd.edu) Web-based platform (Woo et al., 2019; Wang et al., 2016b; Yang et al., 2013). MN analysis can match MS/MS data against reference molecules, identifying known compounds and clustering ions into families according to their spectrometric similarity (Kim et al., 2020; Naman et al., 2017).

In our study, biscoumarins were targeted for isolation from *C. articulata* based on MS/MS analysis. Herein, we describe the isolation, purification, structure elucidation, MS/MS fragmentation analysis and biological testing of these compounds.

* Corresponding author.
E-mail address: bclark@tju.edu.cn (B.R. Clark).

https://doi.org/10.1016/j.phytochem.2021.112856
Received 30 March 2021; Received in revised form 16 June 2021; Accepted 25 June 2021
Available online 6 July 2021

2. Results and discussion

The *n*-BuOH fraction (Figure S1 of Supporting Information) of a methanol extract of *C. articulata* was subjected to untargeted LC-MS/MS analysis. Analysis of MS/MS data with the GNPS database gave 21 tentative hits to known compounds. Nine of these corresponded to flavonoids, while a single hit corresponded to the biscoumarin glycoside rutarensin, suggesting flavonoids and coumarins could be part of the chemical composition of *C. articulata*. The ions in one cluster, designated G1 (Fig. 1), shared a common fragment ion: *m/z* 179, which was also observed in the MS^2 spectrum for the hit of the biscoumarin rutatensin (Figure S2 of Supporting Information). Based on their masses, this suggested that these could be previously unreported coumarins or biscoumarins, which were thus targeted for isolation.

Based on the MN-guided isolation, five undescribed biscoumarins (**1–5**) along with two known coumarin glycosides (**6**, **7**) (Fig. 2) were isolated from the *n*-BuOH fraction of the methanolic extract of *C. articulata*. The known compounds were identified as 6′-acetoxy-daphnetin-8-*O*-β-D-glucoside (**6**) and daphnetin-8-*O*-β-D-glucoside (**7**) by the combined analysis of 1D, 2D NMR, HR-ESI-MS, and by comparison with previously reported NMR data (Shakeel-u-Rehman et al., 2010; Zhu et al., 2008).

Compound **1** was isolated as a yellow amorphous powder. The molecular formula was determined to be $C_{27}H_{24}O_{14}$ due to the observation of an [M - H]$^-$ quasi-molecular ion at *m/z* 571.1080 in the HR-ESI-MS. The ^{1}H-NMR spectrum showed the presence of seven aromatic ^{1}H resonances. The doublet proton signals at δ 6.42 (1H, d, J = 9.6 Hz) and 8.03 (1H, d, J = 9.6 Hz) were characteristic of H-3′ and H-4′ of a coumarin moiety, respectively (Wang et al., 2016a). Another pair of aromatic proton signals at δ 7.44 (1H, d, J = 8.9 Hz), and 7.10 (1H, m) were assigned as H-5′ and H-6′, respectively, of the same 7,8-disubstituted coumarin. Three additional aromatic resonances at δ 6.82, 7.12, and 7.49 ppm were assigned as H-4, H-5 and H-8 of a second coumarin group, this one substituted at positions 3, 6 and 7. The presence of the two coumarin groups was supported by observation of two characteristic coumarin CO resonances at 156.8 and 159.3 ppm in the ^{13}C NMR spectrum. The positions of all substituents were supported by COSY correlations, in addition to HMBC and NOESY data (Fig. 3). A key HMBC correlation from the methoxy singlet at δ 3.76 (3H, s) to C-6 (δ 145.8), located this group at C-6 of the trisubstituted coumarin, which was further supported by a NOESY correlation between the methoxy group and H-5 (δ 7.12). An HMBC correlation from H-8 (δ 6.82) to a downfield carbon at 150.4 ppm suggested the presence of an OH group at C-7.

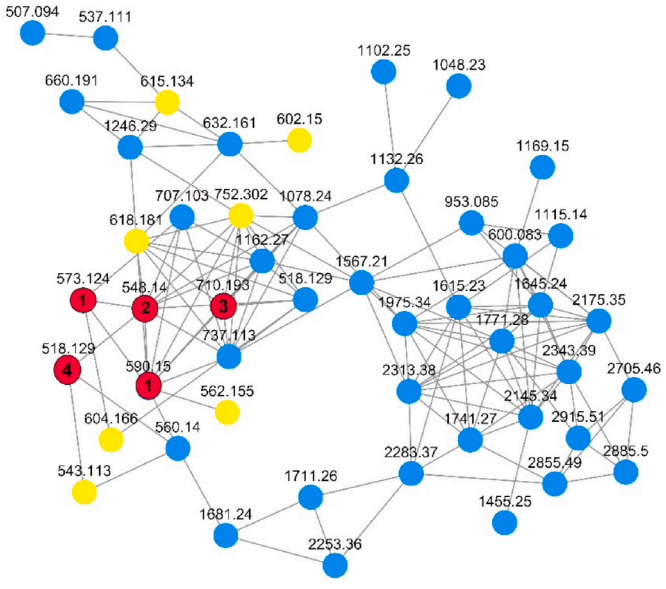

Fig. 1. Molecular network of Cluster G1. Red: Parent ions of isolated new biscoumarins (**1–4**); Yellow: Parent ions for proposed structures. (For interpretation of the references to color in this figure legend, the reader is referred to the Web version of this article.)

For the 7,8-substituted coumarin moiety, substitution was confirmed in a similar manner: COSY, HMBC, and NOESY correlations confirming the locations of the protons at C3′-C6’ (Fig. 3), confirming the presence of substituents at the C-7′ and C-8′ positions. A characteristic anomeric proton signal at δ 5.17 (d, J = 7.6 Hz, H-1″) could be observed in the ^{1}H-NMR spectrum, which correlated to a downfield carbon signal at δ 104.1 in the HSQC spectrum, suggesting the presence of a sugar moiety in compound **1**. A cluster of signals between 3 and 4 ppm in the ^{1}H-NMR, and between 62 and 74 ppm in the ^{13}C-NMR (Table 1), supported this hypothesis and were consistent with the presence of a glucose moiety. Correlations from H-1’’ (δ 5.17) to C-8’ (δ 132.9) in the HMBC spectrum demonstrated that the sugar was located at C-8’. Thus, the linkage between the two coumarin moieties must necessarily be between the C-3 and C-7′ carbons; the C3–*O*–C7′ linkage was supported by the chemical shift of C-3 (δ 137.2); characteristic of a C3–*O*–C7′ linkage (Simões et al., 2009). By further comparison with the data in the literature (Wang et al., 2016a), the aglycone of compound **1** was confirmed to be 6-methoxy-7,8′-hydroxy-3,7′-biscoumarin.

Acid hydrolysis of compound **1**, followed by purification of the resulting sugar, indicated the presence of D-glucose, which was confirmed by comparison of optical rotation ($[\alpha]_D^{25}$ +61.7 (*c* 0.05, H_2O)) and Rf values with a standard sample. The coupling constant (7.6 Hz, H-1″) confirmed the β-configuration of D-glucose (Hernández et al., 2004). Signals consistent with the presence of a single acetate group were observed in both the ^{13}C (δ 169.9, 20.2) and ^{1}H (δ 1.73, 3H) spectra. Correlations from the oxygenated methylene proton H-6’’ (δ 4.03–4.10) with the acetate carbonyl resonance (δ 169.9) in the HMBC spectrum confirmed that the acetyl group was located at C-6″ of the glucose moiety (Fig. 3). Assignment of all glucose signals (Table 1) was supported by the combined analysis of 1D NMR and 2D NMR spectra. Therefore, the structure of compound **1** was determined to be 6″-*O*-acetyl-8′-*O*-β-D-glucopyranosyl-6-methoxy-7-hydroxy-3,7′-biscoumarin (Fig. 2).

Compound **2** was isolated as a yellow amorphous powder. Based a [M - H]$^-$ quasi-molecular ion at *m/z* 529.0981 in the HR-ESI-MS spectrum, the molecular formula was determined to be $C_{25}H_{22}O_{13}$. Comparison of the ^{1}H and ^{13}C NMR spectroscopic data of compounds **2** and **1** (Table 1), suggested the presence of the same 6-methoxy-7-hydroxy-3,7′-biscoumarin aglycone. The NMR data for **1** and **2** were mostly identical, except for the loss of the acetyl group in compound **2**. The anomeric proton signal at δ 5.22 (d, J = 7.2 Hz, H-1″) and its corresponding carbon signal at δ 102.3 suggested the occurrence of one sugar moiety, which was confirmed by acid hydrolysis experiments, again indicating the presence of D-glucose. The β configuration of D-glucose was deduced on the basis of a characteristic coupling constant (7.2 Hz) in the ^{1}H-NMR spectrum. HMBC and NOESY correlations confirmed the locations of glucose and methoxy groups were the same as for compound **1**. Thus, compound **2** was identified as 8′-*O*-β-D-glucopyranosyl-6-methoxy-7-hydroxy-3,7′-biscoumarin (Fig. 2).

Compound **3** was obtained as a yellow amorphous powder. The molecular formula was determined to be $C_{31}H_{32}O_{18}$ based on HR-ESI-MS data (*m/z* 691.1502, [M - H]$^-$). On the basis of the ^{1}H and ^{13}C NMR spectroscopic data (Table 1), compound **3** possessed the same central biscoumarin moiety as for compounds **1** and **2**. The difference was that compound **3** possessed two sugar moieties, as shown by observation of two anomeric proton signals at δ 5.24 (d, J = 7.3 Hz, H-1″) and 5.07 (d, J = 6.8 Hz, H-1‴) in the ^{1}H-NMR spectrum. Acid hydrolysis experiments indicated the presence of only D-glucose, suggesting that compound **3** contained two β-D-glucose moieties. HMBC correlations from H-1’’ (δ 5.24) to C-8’ (δ 133.6) and from H-1‴ (δ 5.07) to C-7 (δ 148.4), together with a correlation from δ 5.24 to H-8 in the NOESY spectrum,

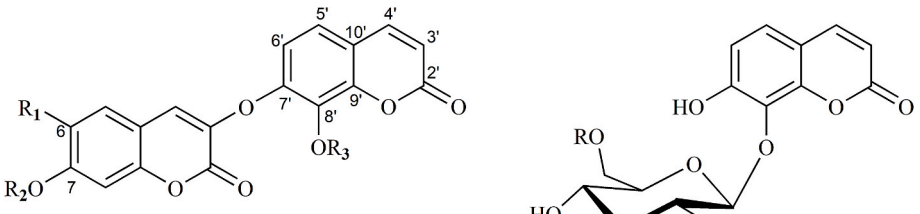

1. R_1=OCH_3; R_2=H; R_3=6-acetyl-*β*-D-Glc
2. R_1=OCH_3; R_2=H; R_3=*β*-D-Glc
3. R_1=OCH_3; R_2=R_3=*β*-D-Glc
4. R_1=H; R_2=H; R_3=*β*-D-Glc
5. R_1=OCH_3; R_2=H; R_3=H

6. R=Ac
7. R=H

Fig. 2. Chemical structures of compounds **1**–**7**.

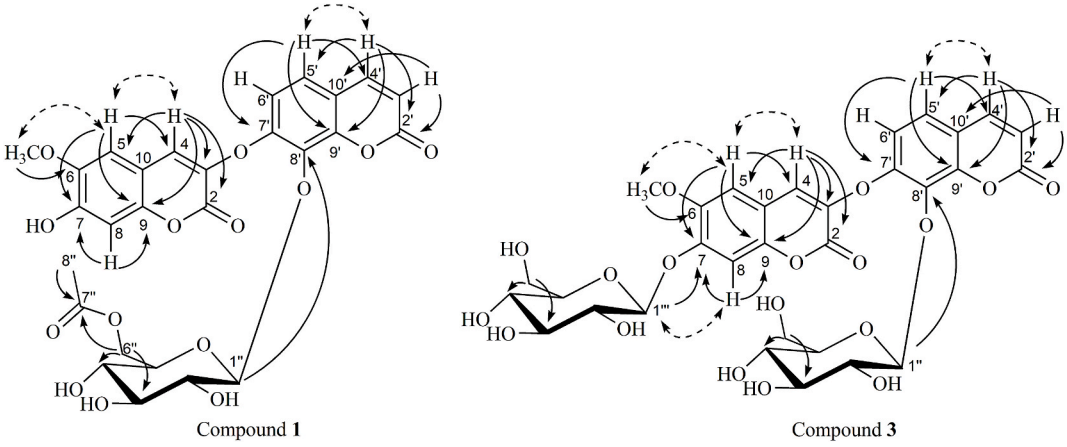

Compound **1** Compound **3**

Fig. 3. Selected HMBC (solid arrows) and NOESY (dashed arrows) correlations for compounds **1** and **3**.

confirmed that the two β-D-glucose moieties were located at C-8′ and C-7 of the biscoumarin moiety (Fig. 3). All signals were assigned by 1D and 2D NMR spectroscopic analysis. Overall, the structure of compound **3** was determined to be 7, 8′-*O*-β-D-diglucopyranosyl-6-methoxy-3,7′-biscoumarin (Fig. 2).

Compound **4** was isolated as a yellow amorphous powder. The molecular formula was determined to be $C_{24}H_{20}O_{12}$ based on HR-ESI-MS data (*m/z* 499.0879, [M - H]$^-$). The ^{1}H and ^{13}C NMR data (Table 1) showed that compound **4** possessed a different aglycone, lacking the 6-OMe group of compounds **1**–**3**. The ^{1}H NMR spectrum showed one typical anomeric sugar proton signal at *δ* 5.20 (d, *J* = 7.4 Hz, H-1″) which correlated to a carbon signal at *δ* 102.4 (C-1″) in the HSQC spectrum. As for the previous compounds, acid hydrolysis confirmed the presence of D-glucose. In the HMBC spectrum, correlations from H-1'' (*δ* 5.20) to C-8' (*δ* 132.9) confirmed that the β-D-glucose moiety was located at C-8′ of the biscoumarin moiety (Fig. 2). All signals were assigned by analysis of 1D and 2D NMR spectra, and the structure of **4** was determined to be 8′-*O*-β-D-glucopyranosyl-7-hydroxy-3,7′-biscoumarin (Fig. 2).

Compound **5** was obtained as a white amorphous powder. Based on a [M - H]$^-$ quasi-molecular ion at *m/z* 367.0449 in the HR-ESI-MS spectrum, the molecular formula was determined to be $C_{19}H_{12}O_8$. The spectroscopic features suggested that its skeleton was the same as for compounds **1**–**3**. However, no signals corresponding to a sugar were observed. Instead, an additional hydroxy group at *δ* 10.19 (br, s) was located at C-8'. Correlations from methoxy group protons at *δ* 3.75 to C-6 (*δ* 145.6) in the HMBC spectrum and correlations from 3.75 (s) to H-5 (*δ* 7.16) in the NOESY spectrum indicated that methoxy group was located at C-6 of the biscoumarin moiety. Thus, the structure of **5** was determined to be 6-methoxy-7,8′-dihydroxy-3,7′-biscoumarin (Fig. 2), the aglycone for compounds **1**–**3**.

MS/MS analysis, in positive mode, revealed that compounds **1**–**7** shared similar fragment ions (Figures S3 of Supporting Information). A fragmentation pathway for these biscoumarins was proposed based on the MS/MS data (Fig. 4). For compound **1** in positive mode, the parent ion at *m/z* 591.1504 can lose a 6′-acetoxy-β-D-glucopyranoside unit to yield a biscoumarin fragment ion at *m/z* 369.0602, which is consistent with the structure of the aglycone **5**. Subsequently, this biscoumarin fragment can split into two different coumarin monomer ions at *m/z* 179.0339 and *m/z* 208.0367, which follow different subsequent fragmentation patterns. The coumarin monomer ion at *m/z* 179.0339 can easily lose a CO group, which is consistent with previous reports (Borkowski et al., 2015; Wang et al., 2014), affording an ion at *m/z* 151.0390. The other ion at *m/z* 208.0367, can lose a methyl group and a CO unit to obtain an ion at *m/z* 164.0104. Compounds **2**, **3** and **5** shared very similar fragmentation patterns with compound **1**. Compound **4**, lacking a 6-OMe group, showed a different fragmentation pattern. The biscoumarin ion at *m/z* 339.0497 indicates the loss of one glucose moiety from the parent ion at *m/z* 518.1290 of compound **4**. Subsequently, the biscoumarin ion can fragment into either of two isomeric coumarin monomer ions, both at *m/z* 179.0339 (Fig. 4). The 7,8-dihydroxylated coumarin fragment can then react in the same way as for compound **1**, losing a CO group and yielding an ion at *m/z* 151.0390, or losing oxygen to give an ion at 163.0389 (Fig. 4). The 3-hydroxylated ion can fragment to form isomeric ions, though it is not possible to determine which of the two pathways predominates. Previous studies have already elucidated possible MS/MS fragmentation pathways for coumarins (Borkowski et al., 2015; Wang et al., 2014) and biscoumarins, which revealed similar fragments (Wang et al., 2016a). MS^2 analysis results indicated that both biscoumarins and coumarin monomers

Table 1
^{1}H (600 MHz) and ^{13}C NMR (150 MHz) data for compounds **1**–**5** in DMSO d_6 (δ (J, Hz)).

Position	1		2	
	H	C	H	C
2		156.8		157.0
3		137.2		137.5
4	7.49 (1H, s)	126.9	7.56 (1H, s)	126.9
5	7.12 (m[a])	109.1	7.12 (m[a])	109.1
6		145.8		145.8
7		150.4		150.3
8	6.82 (1H, s)	102.7	6.81 (1H, s)	102.7
9		146.7		146.7
10		109.8		109.9
6-OMe	3.76 (3H, s)	55.9	3.76 (3H, s)	56.0
2′		159.3		159.4
3′	6.42 (1H, d, 9.6)	114.4	6.42 (1H, d, 9.6)	114.4
4′	8.03 (1H, d, 9.6)	144.2	8.03 (1H, d, 9.6)	144.3
5′	7.44 (1H, d, 8.9)	123.7	7.43 (1H, d, 8.9)	123.5
6′	7.10 (m[a])	114.8	7.09 (m[a])	115.2
7′		150.6		150.7
8′		132.9		133.3
9′		147.8		147.6
10′		115.9		116.0
8′-Glu-1″	5.17 (1H, d, 7.6)	102.3	5.22 (1H, d, 7.2)	102.3
2″	3.20 (m[a])	73.9	3.18 (m[a])	74.0
3″	3.20 (m[a])	76.3	3.18 (m[a])	76.5
4″	3.09 (1H, m)	69.9	3.08 (m[a])	69.7
5″	3.30 (1H, m)	74.1	3.08 (m[a])	77.5
6″	4.03–4.10 (2H, m)	62.8	3.56 (1H, d, 11.0); 3.37 (1H, dd, 4.0, 11.0)	60.6
7″		169.9		
8″-Me	1.73 (3H, s)	20.2		

Position	3		4		5	
	H	C	H	C	H	C
2		156.8		157.2		156.7
3		139.2		135.7		138.3
4	7.50 (1H, s)	124.9	7.65 (1H, s)	128.6	7.34 (1H, s)	124.0
5	7.21 (1H, s)	109.3	7.37 (1H, d, 8.5)	128.9	7.16 (1H, s)	109.1
6		146.3	6.71 (1H, d, 8.5)	114.7		145.6
7		148.4		163.1[b]		149.4
8	7.22 (1H, s)	103.0	6.66 (1H, d, 1.5)	102.3	6.82 (1H, s)	102.6
9		145.7		153.4		146.1
10		112.3		109.3		110.2
6-OMe	3.77 (3H, s)	56.0			3.75 (3H, s)	55.9
7-OH			8.46 (br, s)		10.19 (br, s)	
2′		159.3		159.6		159.7
3′	6.46 (1H, d, 9.5)	114.6	6.40 (1H, d, 9.5)	114.2	6.42 (1H, d, 9.5)	114.5
4′	8.06 (1H, d, 9.5)	144.3	8.01 (1H, d, 9.5)	144.4	8.02 (1H, d, 9.5)	144.6
5′	7.47 (1H, d, 8.6)	123.6	7.40 (1H, d, 8.6)	123.5	7.18 (1H, d, 8.6)	118.5
6′	7.17 (1H, d, 8.6)	115.9	7.07 (1H, d, 8.6)	114.7	7.05 (1H, d, 8.6)	115.5
7′		150.0		151.5		145.6
8′		133.6		132.9		135.7
9′		147.5		147.6		143.9
10′		116.4		115.6		116.3
8′-Glu-1″	5.24 (1H, d, 7.3)	102.3	5.20 (1H, d, 7.4)	102.4		
2″	3.15–3.19 (m[a])	74.0	3.17–3.22 (m[a])	74.0		
3″	3.10 (m[a])	77.4		76.5		
4″	3.10 (m[a])	69.6	3.17–3.22 (m[a]) 3.08–3.09 (m[a])	69.8		
5″	3.15–3.19 (m[a])	76.5	3.08–3.09 (m[a])	77.4		
6″	3.70 (1H, d, 10.5); 3.39–3.47 (m[a])	60.7	3.56 (m[a]); 3.36–3.38 (m[a])	62.7		
7-Glu-1‴	5.07 (1H, d, 6.8)	99.8				
2‴	3.28–3.33 (m[a])	73.1				
3‴	3.39–3.47 (m[a])	77.1				
4‴	3.15–3.19 (m[a])	69.7				
5‴	3.28–3.33 (m[a])	76.8				
6‴	3.56 (1H, d, 14.4); 3.39–3.47 (m[a])	60.6				

[a] Multiplicity undetermined due to overlapping signals.
[b] Observed only in HMBC spectrum; br-broad.

shared a common fragment ion at *m/z* 179. This, combined with the molecular networking (MN) analysis, providing an opportunity to further explore the molecular structures of the remaining coumarins in the molecular network. Based on parent ions and fragmentation patterns, we have proposed some tentative molecular structures for other parent ions observed in cluster G1 (Figures S4 and S5 of Supporting Information), though it should be noted that definitive assignment of positional isomers is not usually possible with MS/MS data alone (Leber et al., 2020). No ions corresponding to daphnoretin itself was not detected in the molecular network, nor in the LC-MS/MS data.

Biscoumarins are a relatively uncommon structure class, in which the two coumarin moieties can be linked in a variety of ways, including simple O- or C-linkages (Tanemossu et al., 2014), or more complex linkages involving spiro centers or isoprenoid linkers (Hussain et al., 2012). While a small number of 3,7′-O-linked biscoumarins have been previously reported in the literature, this is the first report of biscoumarins hydroxylated at the 8′-position. One of the best-known 3, 7′-O-linked biscoumarins is daphnoretin (Cordell, 1984), the structure of which was first proposed in 1963 (Tschesche et al., 1963). Previous studies have showed that daphnoretin possesses multiple biological properties such as anti-tumor, antiviral, and antioxidant activities, and the ability to activate PKC (Deiana et al., 2003; Hussain et al., 2012; Yang et al., 2014). There are very few reports of more-closely related natural products to compounds **1**–**5** in the literature: the only similar compounds with 8′-sustituents are a group of bi- and tri-coumarins incorporating 8′-methoxy groups, reported from *Chimonanthus salicifolius* (Wang et al., 2016a).

Compounds **1**–**7** were tested for a range of biological activities: cytotoxicity against HeLa, MDA-MB-231, HepG2 and MCF-7 cell lines; anti-inflammatory activity *via* inhibition of NO production in RAW264.7 cells; antimicrobial activity against a small suite of test microbes; and α-glucosidase inhibition. For the antibacterial assay, at 40 μg per well (20 μL, 2 mg/mL), none of the compounds showed any growth inhibition against multiple test microbes. For the cytotoxicity assay, anti-inflammatory activity and α-glucosidase inhibitory assay, none of the compounds **1**–**7** showed any inhibition activity at a final concentration of 200 μM. None of the compounds showed activity in any of these assays. Given the reports of cytotoxic properties in other

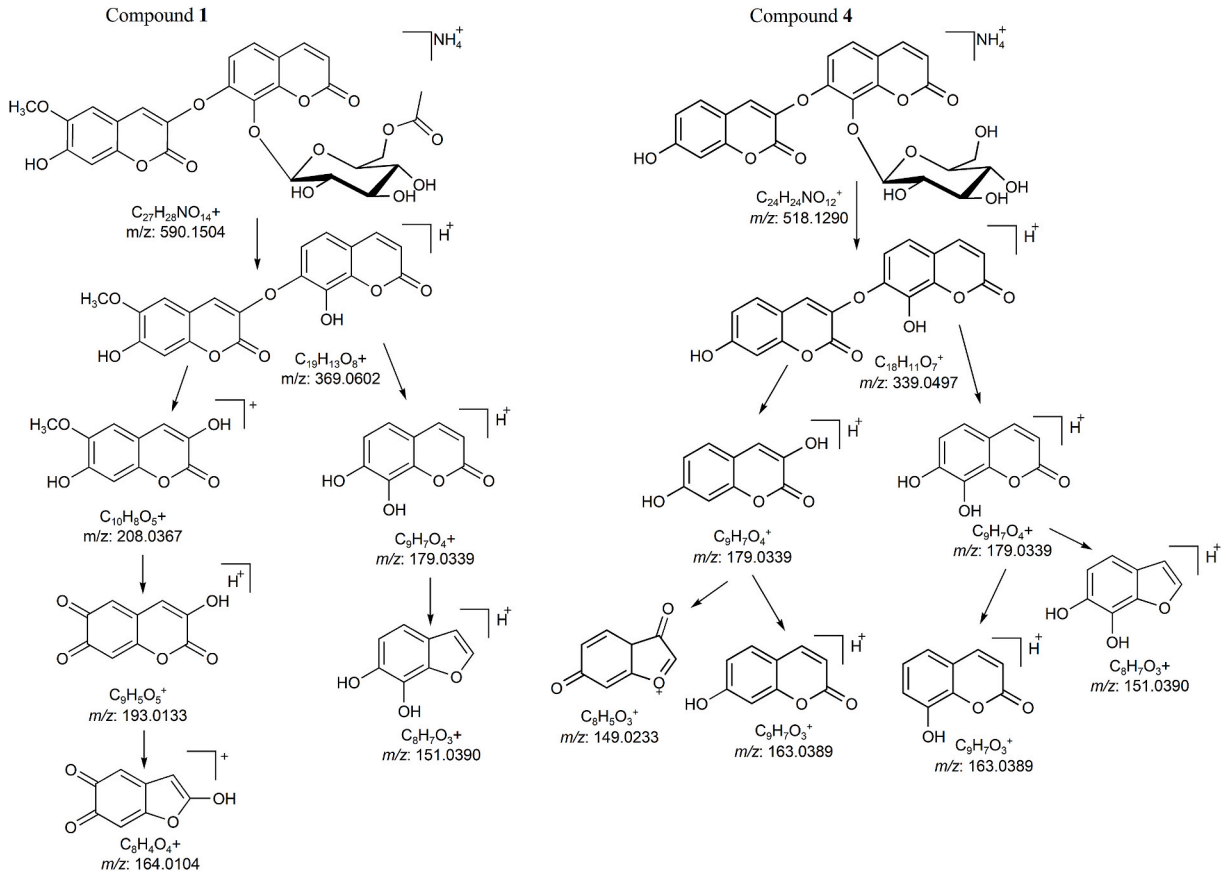

Fig. 4. Proposed fragmentation pathway of compounds **1** and **4**; positive mode.

biscoumarins, the absence of cytotoxic activity for compounds **1**–**7** was unexpected; the presence of the additional OH or glycoside group at position 8′ may reduce the activity of these compounds.

Based on the guidance of MN analysis, we have successfully isolated seven coumarin derivatives from *Cruciata articulata*, five of which were undescribed biscoumarins. The presence of five new biscoumarins, along with 6′-acetoxy-daphnetin-β-D-glucoside (**6**) and daphnetin-8-*O*-glucoside (**7**), constitutes the first description of coumarins and biscoumarins from this species. Though several coumarins have already been reported from the Rubiaceae family (Benevides et al., 2004; Buathong et al., 2019; Dao et al., 2015; De Rosa et al., 2002; Farid et al., 2002; Mfonku et al., 2020; Ralambonirina Rasoarivelo et al., 2018; Singh and Sharma, 2020; Wolff et al., 2019), most of them are coumarin monomers. Biscoumarins are not common in this family, and this is the first time that 3,7′-biscoumarins have been found in the family Rubiaceae; these are also the first biscoumarins to be reported which are glycosylated at the 8′ position. On the basis of MS^2 fragmentation pathway analysis, we have proposed potential structures for some of the minor biscoumarin glycosides appearing in the cluster G1 (Figure S5). According to analysis of the G1 cluster (Fig. 1), there are still several remaining coumarins that have not been isolated and identified, suggesting that *C. articulata* could be further studied in order to expand the knowledge of the phytochemistry of this under-studied species, and to expand the known chemical diversity of biscoumarin derivatives.

3. Experimental

3.1. General

Melting points were measured on a Micro-melting point apparatus with corrections. Optical rotations were recorded on an AUTOPOL II Polarimeter (Rudolph Research Analytical, Hackettstown, NJ, USA). UV–vis spectra were measured using a HITACHI U3900 spectrophotometer (HITACHI, Kyoto, Japan). High-resolution electrospray ionization mass spectra (HR-ESI-MS) were measured using a Q Exactive HF Orbitrap LC-MS (Thermo Fisher Scientific, Waltham MA, USA). NMR spectra were recorded on an Avance III 600 MHz spectrometer (Bruker BioSpin, Billerica MA, USA) using TMS or the residual solvents as internal standard. For open column chromatography, Diaion HP-20 (Mitsubishi Chemical Industries, Tokyo, Japan) was used. Analytical and semipreparative HPLC separations were performed on an Agilent 1260 series HPLC system (G1311B quaternary pump, G1329B autosampler, G1316A thermostatted column compartment and G1315D photodiode array detector; Agilent Technologies, Santa Clara CA, USA), using a Pursuit XRs C18 column (5 μm, 4.6 × 150 mm, Agilent Technologies, USA). Semipreparative HPLC separation was carried out on a Shimadzu LC-20AR series HPLC instrument equipped with a UV detector and a reversed-phase C18 column (Pursuit XRs-C18, 10 μm, 21.2 × 250 mm). All solvents used were of HPLC grade (Concord Technologies, Tianjin, China). Thin-layer chromatography (TLC) was carried out on silica gel GF_{254} plates (Haiyang Chemicals Corp., Qingdao, China). TLC spots were visualized by heating silica gel plates sprayed with 5% H_2SO_4 in EtOH (v/v). The living HeLa, MCF-7 and RAW264.7 cells were purchased from Type Culture Collection of the Chinese Academy of Sciences (Shanghai, China). α-Glucosidase from *Saccharomyces cerevisiae*, acarbose and *p*-nitrophenyl-α-glucopyranoside (PNPG) were purchased from Sigma-Aldrich (St. Louis, MO, USA).

3.2. Plant material

Samples comprising entire plants of *Cruciata articulata* (L.) Ehrend, (Rubiaceae) were collected at Kosmalyan Village near Zarin Gala in the Lerik District of Azerbaijan (38.680310 N, 48.370432 E, 1412 m elevation) in August 2006. Herbarium specimens documenting the

collection (Kerimov 58) have been deposited in the herbaria of the Institute of Botany, Azerbaijan National Academy of Sciences (BAK) and the New York Botanical Garden (NY). The whole plant, including roots, was freed of extraneous matter and air dried in the shade prior to being milled to a coarse powder.

3.3. LC-MS/MS-based molecular networking analysis

A Q Exactive HF orbitrap mass spectrometer coupled with an Ultimate 3000 RSLC nano (Thermo Fisher Scientific, USA) was used for LC-MS/MS analysis in both positive and negative ion modes. An ODS column (Pursuit XRs C18, 5 μm, 4.6 mm × 150 mm, Agilent Technologies, USA) was used for LC separation. The separation was performed as follows: isocratic elution of 23% MeCN for 25 min and then ramping up to 100% MeCN from 25 min to 40 min. Mass resolutions of 120,000 and 30,000 were applied for precursors and fragments. Data dependent MS/MS acquisition with fragmentation of the top five most intense precursors was performed in the analysis. MS/MS spectra were acquired with stepped normalized collision energies (NCE) of 20, 40 and 60. Ion source parameters are as follows: spray voltage, 3.8 kV for positive; capillary temperature, 250 °C; sheath gas flow rate, 45; aux gas flow rate, 12; probe heater temperature, 300 °C; mass range (*m/z*), 100–1500. The data processing of LC-MS/MS raw data was performed using MSConvert software. A molecular network was created using the GNPS Web platform (https://gnps.ucsd.edu). All the results and parameters could be accessed with the GNPS job id for MN analysis (http://gnps.ucsd.edu/ProteoSAFe/status.jsp?task=e5add1d3da2e45fa8f46d93775a03119).

3.4. Extraction and isolation

A 1 kg sample of the dried and powdered plant material was extracted with 3 × 4 L of methanol (MeOH) at ambient temperature (24 h each time), and plant material was macerated without stirring. The pooled methanol extracts were evaporated to dryness *in vacuo* to afford a tarry residue. Then, the methanolic extract (56.8 g) was dispersed in MeOH:H_2O (9:1, 50 mL) and defatted with *n*-hexane (3 × 100 mL), which yielded the *n*-hexane fraction. The hydro-alcoholic phase was freed of solvent, dispersed in water and successively extracted with dichloromethane (DCM) and *n*-BuOH (each 3 × 100 mL) to afford *n*-hexane (1.5 g), DCM (2.2 g), *n*-BuOH (14.5 g) and water (26.5 g) fractions.

The *n*-BuOH fraction (14.5 g) was subject to open column chromatography on Diaion HP-20 (120 g), eluting with a H_2O–MeOH step gradient (each 3 × 200 mL) to give sub-fractions H_2O (2.1 g), 20% MeOH–H_2O (1.4 g), 50% MeOH–H_2O (0.8 g), 80% MeOH–H_2O (6.7 g), 100% MeOH–H_2O (0.4 g), successively. Losses during purification are attributed to imperfect dryness of the initial sample.

The 80% MeOH–H_2O fraction (6.7 g) was separated on a semi-preparative HPLC (Pursuit XRs-C18, 10 μm, 21.2 × 250 mm) at a flow rate of 10 mL/min, by using isocratic elution of 20% MeCN–H_2O for the first 40 min, with subsequent washing with 100% MeCN, which afforded fractions 1–9.

Fraction 5 (0.8 g; t_R 20.00–30.00 min) was separated on a preparative RP-18 column (10 μm, 21.2 × 250 mm, 10 mL/min) using H_2O–MeCN (83:17, v/v), which afforded compound **2** (10.5 mg; t_R 90.0 min), compound **4** (5.6 mg; t_R 84.7 min). Similarly, fraction 3 (0.7 g; t_R 15.00–20.00 min) was fractionated using the same RP-18 column by using 15% MeCN–H_2O with a flow rate at 10 mL/min, and afforded compound **6** (6.2 mg; t_R 48.4 min). Fraction 9 (0.5 g; t_R 42.50–55.00 min) was separated on the RP-18 column using 25% MeCN–H_2O of a flow rate at 8 mL/min, yielding compound **1** (6.8 mg; t_R 29.3 min).

The 20% MeOH–H_2O fraction (1.4 g), together with the 50% MeOH–H_2O fraction (0.8 g) were combined, then separated on a RP-18 column (10 μm, 21.2 × 250 mm, 10 mL/min) using 12% MeCN–H_2O, and affording compounds **3** (11.5 mg; t_R 68.2 min) and **7** (8.3 mg; t_R 59.8 min).

The 100% MeOH–H_2O fraction (0.4 g) was separated on preparative RP-18 column (10 μm, 21.2 × 250 mm) using H_2O–MeCN (73:27, v/v) at a flow rate of 10 mL/min and afforded compound **5** (4.8 mg; t_R 90.2 min).

3.4.1. Compound *1*

Yellow, amorphous powder; mp 209–211 °C; $[\alpha]_D^{25}$ -49.9 (c 0.01, MeOH); UV (MeOH) λ_{max} (log ε) 217 (5.15), 314 (3.70); ^{1}H-NMR (Methanol-d_4, 600 MHz), see Table 1; ^{13}C-NMR (Methanol-d_4, 150 MHz), see Table 1; HRESIMS *m/z* 571.1080 [M - H]$^-$ (calcd. for $C_{27}H_{23}O_{14}$, 571.1082).

3.4.2. Compound *2*

Yellow, amorphous powder; mp 210–212 °C; $[\alpha]_D^{25}$ -62.4 (c 0.01, MeOH); UV (MeOH) λ_{max} (log ε) 217 (5.12), 339 (3.60); ^{1}H-NMR (DMSO d_6, 600 MHz), see Table 1; ^{13}C-NMR (DMSO d_6, 150 MHz), see Table 1; HRESIMS *m/z* 529.0981 [M - H]$^-$ (calcd. for $C_{25}H_{21}O_{13}$, 529.0977).

3.4.3. Compound *3*

Yellow, amorphous powder; mp 208–210 °C; $[\alpha]_D^{25}$ -54.3 (c 0.02, MeOH); UV (MeOH) λ_{max} (log ε) 212 (5.11), 344 (3.41); ^{1}H-NMR (DMSO d_6, 600 MHz), see Table 1; ^{13}C-NMR (DMSO d_6, 150 MHz), see Table 1; HRESIMS *m/z* 691.1502 [M - H]$^-$ (calcd. for $C_{31}H_{31}O_{18}$, 691.1505).

3.4.4. Compound *4*

Yellow, amorphous powder; mp 205–206 °C; $[\alpha]_D^{25}$ -45.2 (c 0.05, MeOH); UV (MeOH) λ_{max} (log ε) 212 (4.97), 341 (3.27); ^{1}H-NMR (DMSO d_6, 600 MHz), see Table 1; ^{13}C-NMR (DMSO d_6, 150 MHz), see Table 1; HRESIMS *m/z* 499.0879 [M - H]$^-$ (calcd. for $C_{24}H_{19}O_{12}$, 499.0871).

3.4.5. Compound *5*

White, amorphous powder; mp 202–204 °C; UV (MeOH) λ_{max} (log ε) 212 (4.80), 343 (3.11); ^{1}H-NMR (DMSO d_6, 600 MHz), see Table 1; ^{13}C-NMR (DMSO d_6, 150 MHz), see Table 1; HRESIMS *m/z* 367.0449 [M - H]$^-$ (calcd. for $C_{19}H_{11}O_8$, 367.0448).

3.4.6. Acid hydrolysis of *1*–*4* and sugar analysis

A solution of each of compounds **1**–**4** (2 mg) in 3% HCl (2 mL) was heated for 4 h. Then, the solution was evaporated several times to dryness with methanol until neutral. The neutralized solutions were centrifuged, filtrated and further purified on a LC-2030 C Prominence-I system (Shimadzu, Kyoto, Japan) equipped with a RID-20 A refractive index detector, using a Waters XBridge BEH Amide column (10 × 250 mm, 5 μm). The flow rate was 3 mL/min, and the mobile phase was MeCN–H_2O (75:25) (Zhao et al., 2019; Liu et al., 2021). The identity of D-glucose was confirmed by comparison of optical rotations with authentic samples (D-glucose, sample: $[\alpha]_D^{25}$ +61.7 (*c* 0.05, H_2O); authentic D-glucose: $[\alpha]_D^{25}$ +61.9 (*c* 0.05, H_2O) and by comparing their TLC behavior with standard samples [Si gel, developed with $CHCl_3$–MeOH–H_2O (8:5:1)] (Zha et al., 2015), both the test sugar and authentic D-glucose shared the same Rf value at 0.35.

3.4.7. Antimicrobial testing

Antimicrobial assays were carried out according to literature protocols (Li and Clark, 2020) against the following test microbes: *Staphylococcus aureus* (ATCC 12600), *Pseudomonas fluorescens* (ATCC 13525), *Enterococcus hirae* (ATCC 8043), *Streptococcus mutans* (ATCC 25175), *Moraxella catarrhalis* (ATCC 25238), *Staphylococcus epidermidis* (ATCC 14990), *Pseudomonas aeruginosa* (ATCC 15692), *Bacillus subtilis* (ATCC

6633), *Saccharomyces kudriavzevii* (ATCC 2601) and *Candida albicans* (ATCC 76615).

3.4.8. Cytotoxicity assay

The cytotoxicity assay was run against MCF-7 (human breast adenocarcinoma cell line), MDA-MB-231 (Human breast cancer cells), HepG2 (Human hepatocellular liver carcinoma) and HeLa (human cervical carcinoma) cell lines using the MTT colorimetric method (Rozimamat et al., 2018), using taxol as a positive control. Cell lines were cultured in DMEM (Corning, USA). All media were supplemented with 10% fetal bovine serum (FBS), 100 U/mL penicillin and 100 μg/mL streptomycin and grown in humidified 5% CO_2 at 37 °C. The test compounds **1**–**7** were dissolved in water and stored as a stock solution at 4 °C. Cells were cultured in 96-well plates at a density of 1×10^4 cells per well in 100 μL medium. After cultivation for 24 h, cells were treated with 100 μL of test compounds at final concentrations of 200 μM, and cultivated for another 24 h. Then, 100 μL of MTT solution prepared at 0.5 mg/mL in phosphate buffered saline was added to each well and incubated for 4 h, after which the contents in each well was discarded and 150 μL of DMSO was added into each well. Absorbance was read on a microplate reader at 490 nm.

3.4.9. Anti-inflammatory activity and NO production

The experiment was conducted according to previous methods, with minor modifications (Cao et al., 2013). Briefly, RAW264.7 macrophages cells were cultured in 96-well plates at 37 °C for 24 h under humidified 5% CO_2 atmosphere. The cells were treated with LPS (1.0 μg/mL) together with the compounds **1**–**7** at a concentration of 200 μM for 24 h. The NO concentration in the culture supernatant was measured by NO assay kit (Microwell plate method, Nanjing Jiancheng Bioengineering Institute, China). Dexamethasone was used as a positive control. Absorbance was recorded at 540 nm on a microplate reader.

3.4.10. Assay for α-glucosidase inhibitory activity

The α-glucosidase inhibitory activity was conducted according to literature procedures, with minor modifications (Fan et al., 2010). Briefly, the reaction mixture consisted of 15 μl of 0.1 M phosphate buffer (pH 6.86), 40 μL of enzyme solution (0.5 U/mL α-glucosidase in 0.1 M phosphate buffer), 5 μL of the indicated concentration of acarbose, or compounds **1**–**7**, in DMSO. The mixture was incubated at 37 °C for 10 min. After this, the reaction was initiated by adding 40 μL of 1.0 mM α-PNPG in 0.1 M phosphate buffer, and incubated 30 min at 37 °C, the reaction was stopped by adding 100 μL of 0.2 M Na_2CO_3. The amount of PNP released was recorded on the microplate reader at 405 nm.

Declaration of competing interest

The authors declare that they have no known competing financial interests or personal relationships that could have appeared to influence the work reported in this paper.

Acknowledgement

This work was funded in part by an award from the National Basic Research Program of China (2015CB856500), and by startup funds from Tianjin University. The authors also acknowledge Y. Gao at the analytical center of the School of Pharmaceutical Science and Technology for their assistance in the acquisition of MS/MS data.

Appendix A. Supplementary data

Supplementary data to this article can be found online at https://doi.org/10.1016/j.phytochem.2021.112856.

References

Abdel-Khalik, K.N., Bakker, F.T., 2007. *Nasturtiopsis integrifolia* (Boulos) Abdel Khalik & Bakker (Brassicaceae), a new combination, and *Cruciata articulata* (L.) Ehrend. (Rubiaceae), a new record for the flora of Egypt. Turk. J. Bot. 31, 571–574.

Aron, A.T., Gentry, E.C., McPhail, K.L., Nothias, L.F., Nothias-Esposito, M., Bouslimani, A., Petras, D., Gauglitz, J.M., Sikora, N., Vargas, F., van der Hooft, J.J.J., Ernst, M., Kang, K. Bin, Aceves, C.M., Caraballo-Rodríguez, A.M., Koester, I., Weldon, K.C., Bertrand, S., Roullier, C., Sun, K., Tehan, R.M., Boya P, C.A., Christian, M.H., Gutiérrez, M., Ulloa, A.M., Tejeda Mora, J.A., Mojica-Flores, R., Lakey-Beitia, J., Vásquez-Chaves, V., Zhang, Y., Calderón, A.I., Tayler, N., Keyzers, R.A., Tugizimana, F., Ndlovu, N., Aksenov, A.A., Jarmusch, A.K., Schmid, R., Truman, A.W., Bandeira, N., Wang, M., Dorrestein, P.C., 2020. Reproducible molecular networking of untargeted mass spectrometry data using GNPS. Nat. Protoc. 15, 1954–1991. https://doi.org/10.1038/s41596-020-0317-5.

Benevides, P.J.C., Young, M.C.M., Da Silva Bolzani, V., 2004. Biological activities of constituents from *Psychotria spectabilis*. Pharm. Biol. 42, 565–569. https://doi.org/10.1080/13880200490901780.

Borkowski, E.J., Cecati, F.M., Suvire, F.D., Ruiz, D.M., Ardanaz, C.E., Romanelli, G.P., Enriz, R.D., 2015. Mass spectrometry and theoretical calculations about the loss of methyl radical from methoxilated coumarins. J. Mol. Struct. 1093, 49–58. https://doi.org/10.1016/j.molstruc.2015.03.007.

Buathong, R., Schindler, F., Schinnerl, J., Valant-Vetschera, K., Bacher, M., Potthast, A., Rosenau, T., Vajrodaya, S., 2019. Uncommon fatty acids, iridoids and other secondary metabolites from the medicinal plant species *Ixora cibdela* Craib (Rubiaceae). Phytochem. Lett. 33, 77–80. https://doi.org/10.1016/j.phytol.2019.07.011.

Cao, G.Y., Yang, X.W., Xu, W., Li, F., 2013. New inhibitors of nitric oxide production from the seeds of *Myristica fragrans*. Food Chem. Toxicol. 62, 167–171. https://doi.org/10.1016/j.fct.2013.08.046.

Chougala, B.M., Samundeeswari, S., Holiyachi, M., Naik, N.S., Shastri, L.A., Dodamani, S., Jalalpure, S., Dixit, S.R., Joshi, S.D., Sunagar, V.A., 2018. Green, unexpected synthesis of bis-coumarin derivatives as potent anti-bacterial and anti-inflammatory agents. Eur. J. Med. Chem. 143, 1744–1756. https://doi.org/10.1016/j.ejmech.2017.10.072.

Cordell, G.A., 1984. Studies in the Thymelaeaceae i. NMR spectral assignments of daphnoretin. J. Nat. Prod. 47, 84–88. https://doi.org/10.1021/np50031a010.

da Cunha, M.G., de Cássia Orlandi Sardi, J., Freires, I.A., Franchin, M., Rosalen, P.L., 2020. Antimicrobial, anti-adherence and antibiofilm activity against *Staphylococcus aureus* of a 4-phenyl coumarin derivative isolated from Brazilian geopropolis. Microb. Pathog. 139, 103855. https://doi.org/10.1016/j.micpath.2019.103855.

Dao, P.T.A., Quan, T., Le Mai, N.T.T., 2015. Constituents of the stem of *Nauclea orientalis*. Nat. Prod. Commun. 10, 1901–1903. https://doi.org/10.1177/1934578x1501001122.

De Rosa, S., Mitova, M., Handjieva, N., Calis, I., 2002. Coumarin glucosides from *Cruciata taurica*. Phytochemistry 59, 447–450. https://doi.org/10.1016/S0031-9422(01)00471-X.

De Rosa, S., Mitova, M., Handjieva, N., Ersoz, T., Calis, I., 2003. Aromatic monoterpenoid glycosides from *Cruciata taurica*. Nat. Prod. Res. 17, 109–113. https://doi.org/10.1080/1478641031000103687.

Deiana, M., Rosa, A., Casu, V., Cottiglia, F., Bonsignore, L., Dessì, M.A., 2003. Chemical composition and antioxidant activity of extracts from *Daphne gnidium* L. J. Am. Oil Chem. Soc. 80, 65–70. https://doi.org/10.1007/s11746-003-0652-x.

Ergun, F., Kusmenoglu, S., Asener, B., 1984. High-performance liquid chromatographic determination of iridoids in *Cruciata taurica*. J. Liq. Chromatogr. 7, 1685–1689. https://doi.org/10.1080/01483918408074076.

Fan, P., Terrier, L., Hay, A.E., Marston, A., Hostettmann, K., 2010. Antioxidant and enzyme inhibition activities and chemical profiles of *Polygonum sachalinensis* F. Schmidt ex Maxim (Polygonaceae). Fitoterapia 81, 124–131. https://doi.org/10.1016/j.fitote.2009.08.019.

Farid, H.A.R., Kunert, O., Haslinger, E., Seger, C., 2002. Isolation and structure elucidation of iridoide and coumarin derivatives from *Xeromphis nilotica* (Rubiaceae). Monatshefte fur Chemie 133, 1453–1458. https://doi.org/10.1007/s00706-002-0500-0.

Gaber, M., El-Wakiel, N., El-Baradie, K., Hafez, S., 2019. Chromone Schiff base complexes: synthesis, structural elucidation, molecular modeling, antitumor, antimicrobial, and DNA studies of Co(II), Ni(II), and Cu(II) complexes. J. Iran. Chem. Soc. 16, 169–182. https://doi.org/10.1007/s13738-018-1494-9.

Gangopadhyay, M., Rai, D.K., Brunton, N.P., Gallagher, E., Hossain, M.B., 2016. Antioxidant-guided isolation and mass spectrometric identification of the major polyphenols in barley (*Hordeum vulgare*) grain. Food Chem. 210, 212–220. https://doi.org/10.1016/j.foodchem.2016.04.098.

Greaves, M., 2005. Pharmacogenetics in the management of coumarin anticoagulant therapy: the way forward or an expensive diversion? PLoS Med. 2, 944–945. https://doi.org/10.1371/journal.pmed.0020342.

Hernández, J.C., León, F., Quintana, J., Estévez, F., Bermejo, J., 2004. Icogenin, a new cytotoxic steroidal saponin isolated from *Dracaena draco*. Bioorg. Med. Chem. 12, 4423–4429. https://doi.org/10.1016/j.bmc.2004.06.009.

Hoult, J.R.S., Payá, M., 1996. Pharmacological and biochemical actions of simple coumarins: natural products with therapeutic potential. Gen. Pharmacol. 27, 713–722. https://doi.org/10.1016/0306-3623(95)02112-4.

Hussain, H., Hussain, J., Al-Harrasi, A., Krohn, K., 2012. The chemistry and biology of bicoumarins. Tetrahedron 68, 2553–2578. https://doi.org/10.1016/j.tet.2012.01.035.

Il'Ina, T.V., Kovaleva, A.M., Goryachaya, O.V., Vinogradov, B.A., 2013. Terpenoids and aromatic compounds from essential oils of *Cruciata laevipes* and *C. glabra*. Chem. Nat. Compd. 48, 1106–1108. https://doi.org/10.1007/s10600-013-0482-7.

Jiang, X., Shangguan, M., Lu, Z., Yi, S., Zeng, X., Zhang, Y., Hou, L., 2020. A "turn-on" fluorescent probe based on V-shaped bis-coumarin for detection of hydrazine. Tetrahedron 76, 130921. https://doi.org/10.1016/j.tet.2020.130921.

Kim, H.W., Park, E.J., Cho, H.M., An, J.P., Chin, Y.W., Kim, J., Sung, S.H., Oh, W.K., 2020. Glucose uptake-stimulating galloyl ester triterpenoids from *Castanopsis sieboldii*. J. Nat. Prod. 83, 3093–3101. https://doi.org/10.1021/acs.jnatprod.0c00645.

Knaggs, A.R., 2003. The biosynthesis of shikimate metabolites. Nat. Prod. Rep. 20, 119–136. https://doi.org/10.1039/b100399m.

Leber, C.A., Naman, C.B., Keller, L., Almaliti, J., Caro-Diaz, E.J.E., Glukhov, E., Joseph, V., Sajeevan, T.P., Reyes, A.J., Biggs, J.S., Li, T., Yuan, Y., He, S., Yan, X., Gerwick, W.H., 2020. Applying a chemogeographic strategy for natural product discovery from the marine cyanobacterium *Moorena bouillonii*. Mar. Drugs 18, 1–25. https://doi.org/10.3390/md18100515.

Li, J., Clark, B.R., 2020. Synthesis of natural and unnatural quinolones inhibiting the growth and motility of bacteria. J. Nat. Prod. 83, 3181–3190. https://doi.org/10.1021/acs.jnatprod.0c00865.

Liang, S., Feng, Y., Tian, J.M., Lu, M., Xiong, Z., Zhang, W.D., 2011. Coumarins from *Daphne feddei* and their potential anti-inflammatory activities. J. Asian Nat. Prod. Res. 13, 1074–1080. https://doi.org/10.1080/10286020.2011.621892.

Liu, X., Atha, D., Clark, B.R., Borris, R.P., 2021. Feruloyl sucrose derivatives from the root of *Xerophyllum tenax*. Phytochemistry 185, 112703. https://doi.org/10.1016/j.phytochem.2021.112703.

Liu, Y.P., Yan, G., Xie, Y.T., Lin, T.C., Zhang, W., Li, J., Wu, Y.J., Zhou, J.Y., Fu, Y.H., 2020. Bioactive prenylated coumarins as potential anti-inflammatory and anti-HIV agents from *Clausena lenis*. Bioorg. Chem. 97, 103699. https://doi.org/10.1016/j.bioorg.2020.103699.

Mitova, M.I., Anchev, M.E., Panev, S.G., Handjieva, N.V., Popov, S.S., 1996. Coumarins and iridoids from *Crucianella graeca, Cruciata glabra, Cruciata laevipes* and *Cruciata pedemontana* (Rubiaceae). Z. Naturforsch. C Biosci. 51, 631–634. https://doi.org/10.1515/znc-1996-9-1005.

Mahapatra, A.K., Maiti, K., Sahoo, P., Nandi, P.K., 2013. A new colorimetric and fluorescent bis(coumarin)methylene probe for fluoride ion detection based on the proton transfer signaling mode. J. Lumin. 143, 349–354. https://doi.org/10.1016/j.jlumin.2013.05.002.

Mfonku, N.A., Tadjong, A.T., Kamsu, G.T., Kodjio, N., Ren, J., Mbah, J.A., Gatsing, D., Zhan, J., 2020. Isolation and characterization of antisalmonellal anthraquinones and coumarins from *Morinda lucida* Benth. (Rubiaceae). Phytochem. Lett. 37, 80–84. https://doi.org/10.1007/s11696-020-01460-3.

Mishra, S., Pandey, A., Manvati, S., 2020. Coumarin: an emerging antiviral agent. Heliyon 6, e03217. https://doi.org/10.1016/j.heliyon.2020.e03217.

Naman, C.B., Rattan, R., Nikoulina, S.E., et al., 2017. Integrating molecular networking and biological assays to target the isolation of a cytotoxic cyclic octapeptide, samoamide A, from an American Samoan marine cyanobacterium. J. Nat. Prod. 80, 625–633. https://doi.org/10.1021/acs.jnatprod.6b00907, 2017.

Pierson, J.T., Dumètre, A., Hutter, S., Delmas, F., Laget, M., Finet, J.P., Azas, N., Combes, S., 2010. Synthesis and antiprotozoal activity of 4-arylcoumarins. Eur. J. Med. Chem. 45, 864–869. https://doi.org/10.1016/j.ejmech.2009.10.022.

Ralambonirina Rasoarivelo, T.S., Grougnet, R., Michel, S., Rakotobe Guillou, C., Deguin, B., 2018. Chemical constituents of *Anthospermum perrieri* (Rubiaceae). Biochem. Systemat. Ecol. 80, 29–31. https://doi.org/10.1016/j.bse.2018.06.002.

Rozimamat, R., Hu, R., Aisa, H.A., 2018. New isopimarane diterpenes and nortriterpene with cytotoxic activity from *Ephorbia alatavica Boiss*. Fitoterapia 127, 328–333. https://doi.org/10.1016/j.fitote.2018.02.026.

Salar, U., Nizamani, A., Arshad, F., Khan, K.M., Fakhri, M.I., Perveen, S., Ahmed, N., Choudhary, M.I., 2019. Bis-coumarins; non-cytotoxic selective urease inhibitors and antiglycation agents. Bioorg. Chem. 91, 103170. https://doi.org/10.1016/j.bioorg.2019.103170.

Shakeel-u-Rehman, Khan, R., Bhat, K.A., Raja, A.F., Shawl, A.S., Alam, M.S., 2010. Estudos de isolamento, caracterização e atividade antibacteriana de cumarinas de *Rhododendron lepidotum Wall*. ex *G. Don*, Ericaceae. Brazilian J. Pharmacogn. 20, 886–890. https://doi.org/10.1590/S0102-695X2010005000037.

Simões, K., Du, J., Pessoni, R.A.B., Cardoso-Lopes, E.M., Vivanco, J.M., Stermitz, F.R., Braga, M.R., 2009. Ipomopsin and hymenain, two biscoumarins from seeds of *Hymenaea courbaril*. Phytochem. Lett. 2, 59–62. https://doi.org/10.1016/j.phytol.2008.11.003.

Singh, B., Sharma, R.A., 2020. Indian Morinda species: a review. Phyther. Res. 34, 924–1007. https://doi.org/10.1002/ptr.6579.

Song, X.F., Fan, J., Liu, L., Liu, X.F., Gao, F., 2020. Coumarin derivatives with anticancer activities: an update. Arch. Pharm. (Weinheim) 353, 1–11. https://doi.org/10.1002/ardp.202000025.

Tanemossu, S.A.F., Franke, K., Arnold, N., Schmidt, J., Wabo, H.K., Tane, P., Wessjohann, L.A., 2014. Rare biscoumarin derivatives and flavonoids from *Hypericum riparium*. Phytochemistry 105, 171–177. https://doi.org/10.1016/j.phytochem.2014.05.008.

Tava, A., Biazzi, E., Ronga, D., Avato, P., 2020. Identification of the volatile components of *Galium verum* L. And *Cruciata leavipes* opiz from the western Italian alps. Molecules 25, 1–11. https://doi.org/10.3390/molecules25102333.

Tschesche, R., Schacht, U., Legler, G., 1963. Über Daphnorin, ein neues Cumaringlucosid aus Daphne mezereum. Naturwissenschaften 50, 521–522. https://doi.org/10.1007/BF00689237.

Ushakov, V.B., Kopylova, V.N., Luk'yanchikov, M.S., Melik-Guseinov, V.V., 1988. Anthraquinones of *Gallium articulatum*. Chem. Nat. Compd. 24, 257. https://doi.org/10.1007/BF00596767.

Wang, B., Liu, X., Zhou, A., Meng, M., Li, Q., 2014. Simultaneous analysis of coumarin derivatives in extracts of *Radix Angelicae pubescentis* (Duhuo) by HPLC-DAD-ESI-MS^n technique. Anal. Methods 6, 7996–8002. https://doi.org/10.1039/c4ay01468e.

Wang, K.W., Li, D., Wu, B., Cao, X.J., 2016a. New cytotoxic dimeric and trimeric coumarins from *Chimonanthus salicifolius*. Phytochem. Lett. 16, 115–120. https://doi.org/10.1016/j.phytol.2016.03.009.

Wang, M., Carver, J.J., Phelan, V.V., Sanchez, L.M., Garg, N., Peng, Y., Nguyen, D.D., Watrous, J., Kapono, C.A., Luzzatto-Knaan, T., Porto, C., Bouslimani, A., Melnik, A. V., Meehan, M.J., Liu, W.T., Crüsemann, M., Boudreau, P.D., Esquenazi, E., Sandoval-Calderón, M., Kersten, R.D., Pace, L.A., Quinn, R.A., Duncan, K.R., Hsu, C. C., Floros, D.J., Gavilan, R.G., Kleigrewe, K., Northen, T., Dutton, R.J., Parrot, D., Carlson, E.E., Aigle, B., Michelsen, C.F., Jelsbak, L., Sohlenkamp, C., Pevzner, P., Edlund, A., McLean, J., Piel, J., Murphy, B.T., Gerwick, L., Liaw, C.C., Yang, Y.L., Humpf, H.U., Maansson, M., Keyzers, R.A., Sims, A.C., Johnson, A.R., Sidebottom, A. M., Sedio, B.E., Klitgaard, A., Larson, C.B., Boya, C.A.P., Torres-Mendoza, D., Gonzalez, D.J., Silva, D.B., Marques, L.M., Demarque, D.P., Pociute, E., O'Neill, E.C., Briand, E., Helfrich, E.J.N., Granatosky, E.A., Glukhov, E., Ryffel, F., Houson, H., Mohimani, H., Kharbush, J.J., Zeng, Y., Vorholt, J.A., Kurita, K.L., Charusanti, P., McPhail, K.L., Nielsen, K.F., Vuong, L., Elfeki, M., Traxler, M.F., Engene, N., Koyama, N., Vining, O.B., Baric, R., Silva, R.R., Mascuch, S.J., Tomasi, S., Jenkins, S., Macherla, V., Hoffman, T., Agarwal, V., Williams, P.G., Dai, J., Neupane, R., Gurr, J., Rodríguez, A.M.C., Lamsa, A., Zhang, C., Dorrestein, K., Duggan, B.M., Almaliti, J., Allard, P.M., Phapale, P., Nothias, L.F., Alexandrov, T., Litaudon, M., Wolfender, J. L., Kyle, J.E., Metz, T.O., Peryea, T., Nguyen, D.T., VanLeer, D., Shinn, P., Jadhav, A., Müller, R., Waters, K.M., Shi, W., Liu, X., Zhang, L., Knight, R., Jensen, P.R., Palsson, B., Pogliano, K., Linington, R.G., Gutiérrez, M., Lopes, N.P., Gerwick, W.H., Moore, B.S., Dorrestein, P.C., Bandeira, N., 2016b. Sharing and community curation of mass spectrometry data with global natural products social molecular networking. Nat. Biotechnol. 34, 828–837. https://doi.org/10.1038/nbt.3597.

Watrous, J., Roach, P., Alexandrov, T., Heath, B.S., Yang, J.Y., Kersten, R.D., Van Der Voort, M., Pogliano, K., Gross, H., Raaijmakers, J.M., Moore, B.S., Laskin, J., Bandeira, N., Dorrestein, P.C., 2012. Mass spectral molecular networking of living microbial colonies. Proc. Natl. Acad. Sci. U.S.A. 109, 1743–1752. https://doi.org/10.1073/pnas.1203689109.

Wolff, T., Berrueta, L.A., Valente, L.M.M., Barboza, R.S., Neris, R.L.S., Guimarães-Andrade, I.P., Assunção-Miranda, I., Nascimento, A.C., Gomes, M., Gallo, B., Iriondo, C., 2019. Comprehensive characterisation of polyphenols in leaves and stems of three anti-dengue virus type-2 active *Brazilian Faramea* species (Rubiaceae) by HPLC-DAD-ESI-MS/MS. Phytochem. Anal. 30, 62–72. https://doi.org/10.1002/pca.2790.

Woo, S., Kang, K. Bin, Kim, J., Sung, S.H., 2019. Molecular networking reveals the chemical diversity of selaginellin derivatives, natural phosphodiesterase-4 inhibitors from *Selaginella tamariscina*. J. Nat. Prod. 82, 1820–1830. https://doi.org/10.1021/acs.jnatprod.9b00049.

Yang, J.Y., Sanchez, L.M., Rath, C.M., Liu, X., Boudreau, P.D., Bruns, N., Glukhov, E., Wodtke, A., De Felicio, R., Fenner, A., Wong, W.R., Linington, R.G., Zhang, L., Debonsi, H.M., Gerwick, W.H., Dorrestein, P.C., 2013. Molecular networking as a dereplication strategy. J. Nat. Prod. 76, 1686–1699. https://doi.org/10.1021/np400413s.

Yang, Z.Y., Kan, J.T., Cheng, Z.Y., Wang, X.L., Zhu, Y.Z., Guo, W., 2014. Daphnoretin-induced apoptosis in HeLa cells: a possible mitochondria-dependent pathway. Cytotechnology 66, 51–61. https://doi.org/10.1007/s10616-013-9536-8.

Zha, H., Wang, Z., Yang, X., Jin, D., Hu, L., Zheng, W., Xu, L., Yang, S., 2015. New acylated triterpene saponins from the roots of *Securidaca inappendiculata* Hassk. Phytochem. Lett. 13, 108–113. https://doi.org/10.1016/j.phytol.2015.05.022.

Zhao, P., Zhou, H., Zhao, C., Li, X., Wang, Y., Huang, L., Gao, W., 2019. Purification, characterization and immunomodulatory activity of fructans from *Polygonatum odoratum* and *P. cyrtonema.* Carbohydr. Polym. 214, 44–52. https://doi.org/10.1016/j.carbpol.2019.03.014.

Zhu, Y., Zhao, Y., Huang, G., Du, Wu, W.S., 2008. Four new compounds from *Sinacalia tangutica*. Helv. Chim. Acta 91, 1894–1901. https://doi.org/10.1002/hlca.200890203.